LARGE-SIGNAL NETWORK ANALYSER MEASUREMENTS APPLIED TO BEHAVIOURAL MODEL EXTRACTION

Maciej Myslinski, K.U.Leuven, Div. ESAT-TELEMIC, Kasteelpark Arenberg 10, B-3001 Leuven, Belgium, e-mail: maciej.myslinski@esat.kuleuven.be
Dominique Schreurs, the same institution, e-mail: dominque.schreurs@esat.kuleuven.be
Bart Nauwelaers, the same institution, e-mail: bart.nauwelaers@esat.kuleuven.be

Abstract

Large-signal network analyser (LSNA) measurements provide detailed insight into the behaviour of a measured device under test (DUT) in the presence of realistic excitations. This information has already been used to construct accurate behavioural models of many DUTs regardless the degree of their complexity. Our purpose is to show how to process the LSNA-measured quantities to obtain the independent time-domain variables and on this basis efficiently extract the behavioural model of a given DUT. The method is illustrated with a practical example at circuit level (4.9 GHz buffer amplifier).

I. Introduction

Large-signal network analyser is a broadband and highly dynamic set-up measuring simultaneously the amplitude and phase of all spectral components of the incident and scattered travelling voltage waves of the two-port DUT [1]. The measurement data transformed to time-domain have been successfully used in the non-linear behavioural modelling technique [2]. Regardless the DUT or the application for which the model is predestined, its accuracy and valid operating range relies largely on proper experiment design. In previous studies it was shown that more efficient experiment design and more realistic operation conditions can be achieved by proper signal choice, in particular statistically shaped multisine excitation [3]. It was also demonstrated how to extend the model's operational range to account for better accuracy under various types of excitations [4].

The main problem encountered during measurement-data processing is the large number of time-domain data points, especially in case of modulated signals like the narrow-band multisines. This results from the large difference between the RF carrier frequency (gigahertz range) and the narrow-band multisine frequency offset (tens of kilohertz range) [5]. Therefore in order to save time and resources, as well as maintain high accuracy of the resulting behavioural model, both the number of data points and the sampling method have to be optimised [6].

In this work we explain how to apply LSNA measurements for time-domain behavioural model construction. In Section II the modelling method used in our research is described together with the outline of the extraction procedure. In Section III we discuss the measurement data processing procedure with special attention put to the IF data sampling method. Practical illustration of this modelling approach on the example of a general purpose buffer amplifier

1

designed for modern RF telecommunication applications is presented in Section IV, followed by conclusions in Section V.

II. Large-Signal Time-Domain Behavioural Modelling

The large-signal modelling approach discussed in this work can be classified as a nonlinear time-domain (or state-space) behavioural modelling technique with nonlinear memory [2]. The modelling method is essentially based on the description of a two-port RF device that exhibits no long-term memory effects by the dynamical equations:

$$i_1(t) = f_1(v_1(t), v_2(t), \dot{v}_1(t), \dot{v}_2(t), \ddot{v}_1(t), ... \dot{i}_1(t), \dot{i}_2(t), \ddot{i}_1(t), ...), \tag{1}$$

$$i_2(t) = f_2(v_1(t), v_2(t), \dot{v}_1(t), \dot{v}_2(t), \ddot{v}_1(t), ... \dot{i}_1(t), \dot{i}_2(t), \ddot{i}_1(t), ...), \tag{2}$$

or in equivalent form using travelling voltage waves:

$$b_1(t) = g_1(a_1(t), a_2(t), \dot{a}_1(t), \dot{a}_2(t), ..., \dot{b}_1(t), \dot{b}_2(t), ...), \tag{3}$$

$$b_2(t) = g_2(a_1(t), a_2(t), \dot{a}_1(t), \dot{a}_2(t), ..., \dot{b}_1(t), \dot{b}_2(t), ...). \tag{4}$$

$i_i(t)$, $v_i(t)$ and $b_i(t)$, $a_i(t)$ representing the terminal currents, voltages and the scattered, incident travelling voltage waves respectively. The superscript dots denote (higher-order) time derivatives. Both representations of the dynamical equations using the terminal currents and voltages (1)-(2) and based on travelling voltage waves (3)-(4) are related with each other as follows:

$$a = \frac{v + Z_c i}{2}, b = \frac{v - Z_c i}{2}. \tag{5}$$

In equation (5) Z_c represents characteristic impedance, usually 50 Ohm. Typically the terminal currents and voltages are more convenient to use when the modelled device is a transistor. On the other hand, travelling voltage waves are more convenient in case of model predestined for application on higher-level analysis e.g., circuit or system level.

Regardless the type of quantities applied, the goal of the procedure is to determine the set of independent variables, and subsequently use it to derive the functions $f_1(.)$ and $f_2(.)$ or $g_1(.)$ and $g_2(.)$. The former is usually accomplished by numerical methods based on the false nearest neighbour approach [7]. The functions (1)-(4) can have various forms e.g. polynomials, artificial neural networks (ANN), support vector machines (SVM). Typically, we use an ANN with parameters found by optimization [8], mainly because the constant asymptotic values of the sigmoid activation function prevent rapid error increase during function extrapolation in a simulator [9].

The data required as input to the modelling procedure comes directly from the LSNA measurements or indirectly that is, the higher-order time derivatives are calculated from the measurements. As mentioned in the Introduction, the experiment design, and thus also the measurement plan, essentially determines the valid operating range of the model. Therefore when defining the measurement plan we should take into account the application and the conditions in which the extracted model is expected to work. Very important at this stage is the type of excitation. From the point of view of efficient experiment design, modern wireless applications and the limitation of LSNA to only periodic excitations, we usually use narrowband

multisine signals. Unfortunately, dealing with modulated LSNA data often means reaching the resources limits required to extract the behavioural model. Therefore we need to optimise the generation of the time-domain variables, mainly involving a reduction of the data points without sacrificing the accuracy of the resulting model. In the next section we will present more detailed discussion of the LSNA-data processing procedure.

Finally we combine processed waveforms into the minimal set of the independent time-domain variables used to derive the ANN equations. After the implementation in a commercial circuit simulator, the extracted behavioural model can be used in circuit design and simulation.

III. LSNA Data Processing

Once the LSNA measurement is done, we have access to the instantaneous voltages/currents and travelling voltage waves measured at the ports of the DUT and represented both in time- and frequency- domains. Please note that even if the modelling method requires the independent variables in the time-domain, the processing begins with the frequency-domain data. The main reason is the calculation of time derivatives necessary for model equations (1)-(4). According to the differentiation property of the Fourier transform, calculation of the time derivative of a waveform is equivalent in the frequency-domain to a simple multiplication of its Fourier transform by the imaginary unit j and the angular frequency ω [10]:

$$\text{If } x(t) \leftrightarrow X(f) \text{ then } \dot{x}(t) \leftrightarrow j\omega X(f), \tag{6}$$

where $x(t)$ and $X(f)$ represent time-domain waveform and its corresponding Fourier transform.

Another motivation behind post-processing the LSNA-measured data in the frequency-domain is the ability to increase the oversampling factor of the measured frequency spectra and thus easily improve smoothness of the resulting time-domain waveforms. Finally, applying inverse Fourier transform to the measured spectral data, as well as that modified according to (6), leads to the required time-domain variables from the equations (1)-(4). The waveforms are sampled at time instances defined by the fundamental frequency, the number of harmonics considered and the oversampling factor.

The situation is more complicated when we are moving from single-tone excitations to multisine modulated signals. The general idea of processing the frequency-domain data remains the same with a small modification that all the considered data structures obtain one new dimension related to the modulation frequency and its harmonics. The problems are related to the inverse Fourier transformation of this two-dimensional spectral data with a large difference between the RF carrier and the modulation frequency grids usually in gigahertz and kilohertz range, respectively. The time-domain waveforms are composed now of millions of "short" periods of the RF carrier frequency modulated with one "long" period defined by the modulation frequency. Obviously, such enormous data sets cannot be used in practical applications. Therefore authors in [5] proposed to select only a few "short" periods of the RF carrier frequency along the "long" modulation envelope period. Fig. 1 illustrates this approach. The plots (a) and (b) show instantaneous voltage waveforms measured at the input and output of a DUT excited with a three-tone multisine. Due to the significant difference between the modulation envelope and the RF carrier frequency periods, we cannot see in these plots rapid oscillations of the RF carrier frequency. Grey vertical lines depict 16 RF carrier periods taken equidistantly in time along the envelope period. These RF periods, when plotted against each other create coverage plots, as

3

shown on Fig. 1 (c). Each RF period forms an elliptical trajectory with a shape distorted by the nonlinearity of the DUT.
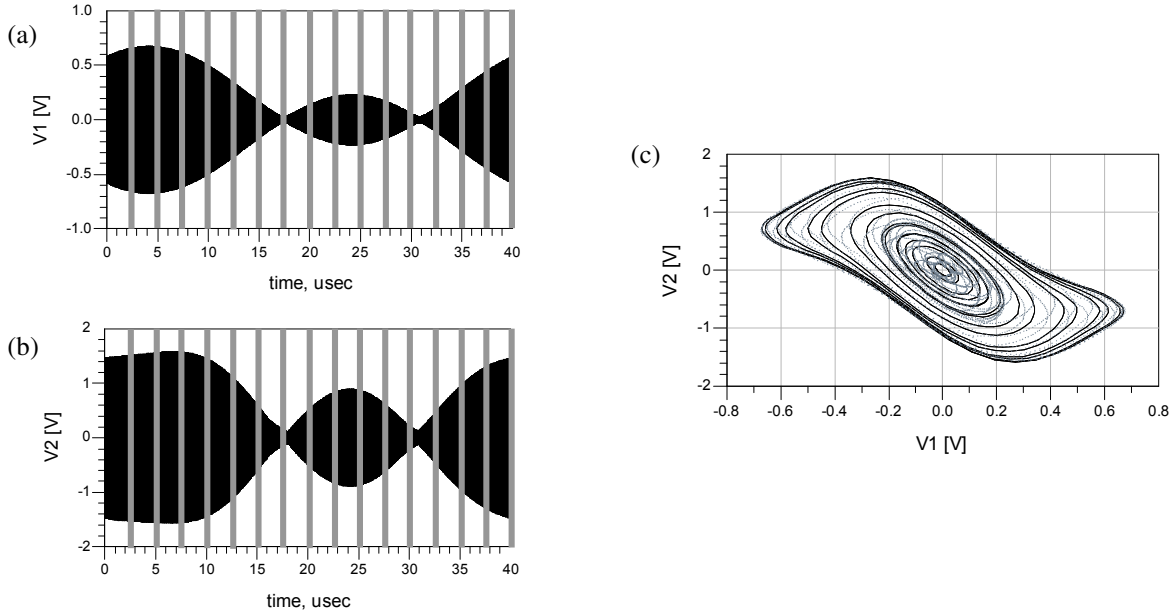

Fig. 1. Instantaneous voltage waves at the input (a) and the output (b) of a DUT excited with a three-tone multisines; (c) (v_2, v_1) coverage plot created by 16 RF periods chosen equidistantly in time from (a) and (b).

The way the trajectories cover the space of the time-domain variables has a direct impact on the validity range of the behavioural model extracted from these data [3]. Knowing that the operational range of measurement-based ANN behavioural models has very limited extrapolation capability [11], one can suggest to increase the number of RF periods taken from the IF envelope period, resulting in denser coverage and thus larger validity range of the model. However, this leads to higher demand for resources and computational time and in consequence to decreased modelling efficiency. Besides, the inability to control shape of the waveforms' envelopes and the nonlinear distortion in the modelled DUT, render uniform coverage of the required operational range of the model very difficult.

A solution to solve this problem has been proposed in [12]. The authors introduced a nonlinearity metric (7) calculated for each RF carrier frequency period and then used this information rather than time-domain distribution to select the trajectories for a model generation. A preference was given to the RF periods associated with higher values of the nonlinearity parameter, what resulted in the improved behavioural model accuracy [12]. Recent studies showed that sampling waveforms in the nonlinearity parameter domain instead of the time-domain leads not only to significant reduction of data sets and more efficient modelling procedure but also improves behavioural model's prediction of DUT's response to different types of signals [6].

Taking all the above into consideration we calculate the nonlinearity metric σ, defined in [6] as:

$$\sigma_k = \sqrt{\frac{1}{N}\sum_{i=1}^{N}\left|X_{ki} - X_{ri}\right|^2}\;,\tag{7}$$

where X_{ki} and X_{ri} represent *k-th* and reference (linear) RF period trajectories, respectively. *N* is the number of samples along *k-th* trajectory. The normalisation involves dividing the instantaneous amplitudes of the output voltage waveform or the output scattered travelling voltage wave by the peak value of $v_1(t)$ or $a_1(t)$ waveform reached in each of the RF periods. It should be mentioned that we have to assure the phase alignment of the RF period trajectories, especially when working with the modulated data. Otherwise we will subtract the samples corresponding to different phases of the RF carrier leading to erroneously high values of the metric (7) even for very linear trajectories.

Subsequently we can plot the nonlinearity parameter σ (7) results obtained for a high number of RF carrier frequency periods in the function of the increasing peak amplitude value, as on Fig. 2 (a). From the plot we identify a threshold value of the nonlinearity metric separating predominantly linear and non-linear RF trajectories. Fig. 2 (b) presents the reduced number of points obtained by selecting from the original set fewer samples below and more samples above the threshold value.
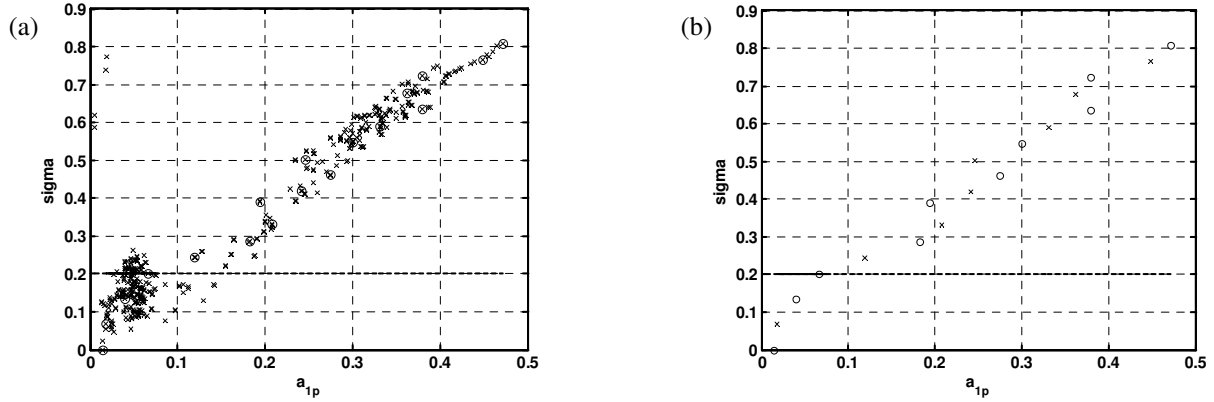

Fig. 2. (a) The nonlinearity metric (7) calculated for 256 (crosses) RF carrier frequency periods of the incident travelling voltage wave measured at the input of a DUT; circles denote 18 RF periods chosen for further data processing [6]; (b) 18 out of 256 samples divided into ANN training (circles) and testing (crosses) data.

This piecewise equidistant sampling in the σ domain influences the RF trajectories distribution on the (b_2, a_1) coverage, as can be seen on Fig. 3 (a) and (b). The graphs show the (b_2, a_1) coverage achieved by 18 RF trajectories chosen according to Fig. 2 (b) and using the uniform sampling in the time-domain as on Fig. 1., respectively. As a result the same number of trajectories can lead to effectively better coverage of model's validity range.

Using similar methodology we also select the corresponding RF carrier trajectories of other time-domain waveforms from the equations (1)-(2) or (3)-(4) to form the set of independent variables for model extraction. Please note that all the above discussion referred to only one LSNA measurement. In most cases the experiment design involves performing multiple measurements for different parameters e.g., input power level, types of excitation, bias conditions, source/load impedance, etc. In this case the described data processing is repeated for each of the considered

measurements. Subsequently the set of time-domain variables can be assembled and used for behavioural model extraction following the procedure outlined in section II.
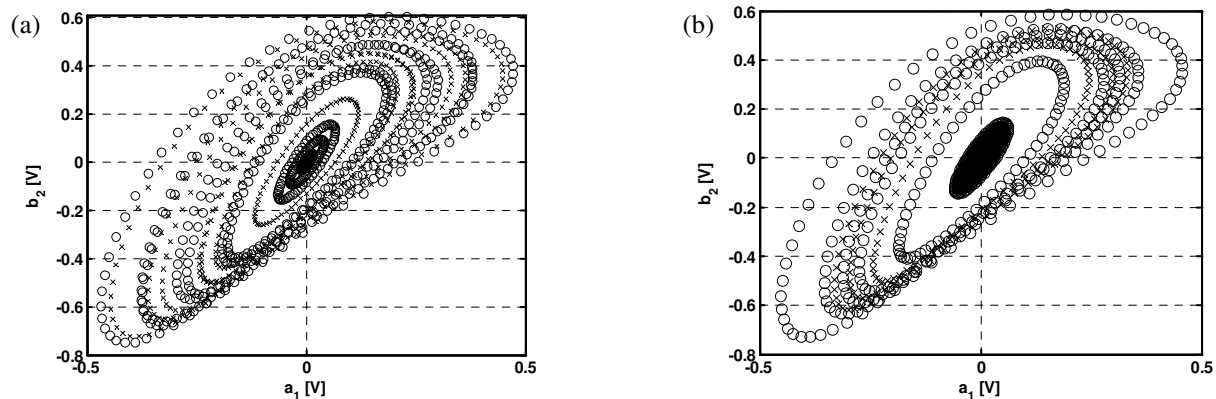

Fig. 3. The (b_2, a_1) coverage plot created by 18 RF periods chosen from the IF envelope period: (a) piecewise equidistantly in the nonlinearity metric σ domain, (b) equidistantly in the time-domain. Circles and crosses depict trajectories used for ANN training and testing, respectively [6].

IV. Practical Example

The large-signal behavioural modelling method has been applied to an off-the-shelf InGaP HBT-based buffer amplifier assembled on an evaluation board and tuned at around 4.9 GHz. The circuit has been measured using the LSNA set-up under large-signal multisine excitation generated at 4.9 GHz. We measured incident and scattered travelling voltage waves, present at the input and output ports of the DUT. The frequency-domain data has been available in 8 MHz band around the RF carrier frequency and up to its 4th harmonic.

We used two types of 63-tone multisine with the amplitudes and phases optimized to approximate the probability density function (PDF) of the 1.6 MHz bandwidth quadrature phase shift keying (QPSK) signal [3]. The multisines were derived from two different realisations of QPSK digitally modulated signal at 4.9 GHz. In both cases the input power was swept from –20 dBm to +6 dBm (at the generator output) with the step of 2 dBm. It should be noted that the losses in the RF cables reduced these levels by 6 dB at the measured ports. The first type of the multisine will be used to extract the model, while the second one will serve for model verification purposes.

After the calculations of the time derivatives performed according to (6), we transformed all the spectral data into the time-domain. For the RF carrier frequency scale we used the oversampling ratio eight, resulting in the total number of 64 RF period samples. In case of the IF modulation envelope period we decided to have 256 samples. Fig. 4 shows one period of the amplitude envelope of the excitation signal. One can notice from the shape of the envelope that it could have twice smaller period than plotted. This is due to the fact that most of the signal's energy is located on every second tone of the multisine.
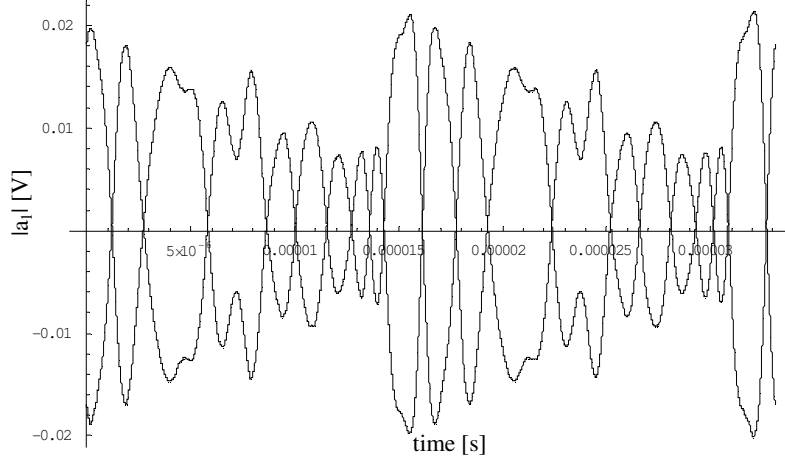
Fig. 4. One period of the amplitude envelope of the input travelling voltage wave.

In order to optimise the number of IF period samples we change sampling domains, as reported in Section III. After calculating the nonlinearity metric σ for 256 RF periods sampled equidistantly in time-domain along the envelope period from Fig. 4, we defined linear and nonlinear regions depending on the σ value lower or higher than 0.2. Fig. 2 (a) depicts this division. For further analysis we select only 18 samples in the way illustrated by Fig. 2 (b). The circles represent ten samples, which will form the training set, while crosses characterise eight trajectories from the future testing set of the ANN. Fig. 3 (a) shows the corresponding (b_2, a_1) coverage.

Subsequently, we select the RF trajectories at two input power levels –10 dBm and +6 dBm providing information about the amplifier's behaviour at lower and higher power levels. Both data sets are combined into the time-domain variables used for the ANN model extraction. It should also be mentioned that using the false nearest neighbour method [7], we obtained the final set of the independent data composed of $a_1(t)$, $a_2(t)$, their time derivatives and also $b_1(t)$ derivative.

Finally, we trained the ANN with one hidden layer of 20 neurons representing the functional relationships (3)-(4). After incorporation into a commercial circuit simulator, we performed simulations basing on the second type of the multisine measurements described earlier in this section. Fig. 5 depicts both the simulation (solid trace) and the measurement (circles) time-domain results of the b_2 scattered traveling voltage wave at port 2 obtained for the considered amplifier. The graphs in Fig. 5 (a) and (b) respectively show the magnitude and phase of the complex envelope around the carrier frequency. Similar results for the complex envelope around the second RF harmonic are plotted on Fig. 3(c) and (d), respectively. The input power of the multisine signal was set to +6 dBm. All these plots reveal a very good agreement between the measurements and the model predictions around the RF carrier frequency as well as around its second harmonic.
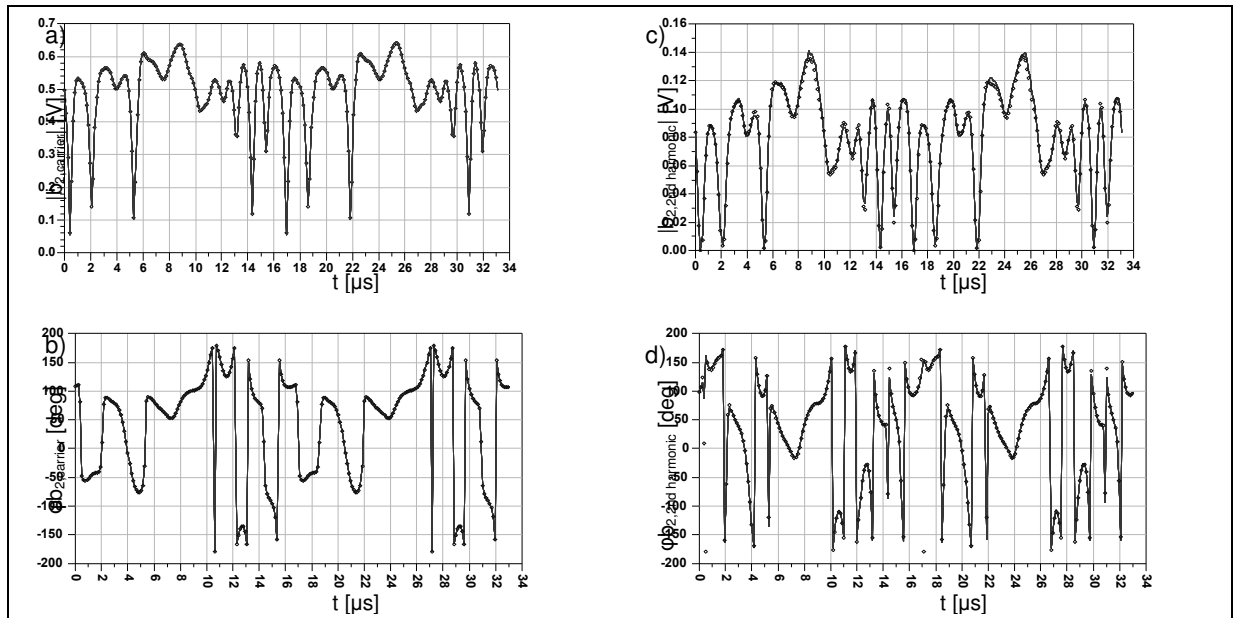
7

Fig. 5. The measured (circles) and simulated (solid trace) b_2 scattered traveling voltage wave: (a) magnitude waveform, (b) phase waveform of the complex envelope around RF carrier frequency 4.9 GHz, and (c) magnitude waveform, (d) phase waveform of the complex envelope around the second RF harmonic; the input power is 6 dBm.

V. Conclusion

In this work we explained the behavioural modelling approach based on LSNA measurements. We discussed in detail the measurement data processing procedure with special attention put to the efficient reduction of the waveform data sets. This methodology was illustrated with a practical example of an off-the-shelf buffer amplifier designed for RF applications. Very good agreement between large-signal measurements and simulations both in amplitude and phase was achieved for the complex envelope not only around the carrier RF frequency but also around its second harmonic.

Acknowledgements

References

[1]   J. Verspecht, P. Debie, A. Barel, and L. Martens, "Accurate on wafer measurements of phase and amplitude of the spectral components of incident and scattered voltage waves at the signal ports of a nonlinear microwave device," *IEEE MTT-S Digest*, pp. 1029-1032, May 1995.

[2]   D. Schreurs, J. Wood, N. Tufillaro, L. Barford, and D. Root, "Construction of behavioural models for microwave devices from time-domain large-signal measurements to speed-up high-level design simulations," International Journal of RF and Microwave Computer Aided Engineering, vol. 13, no. 1, pp. 54-61, 2003.

[3] M. Myslinski, D. Schreurs, K.A. Remley, M.D. Mc Kinley and B. Nauwelaers, "Large-Signal Behavioral Model of a Packaged RF Amplifier Based on QPSK-Like Multisine Measurements", *Proc. of the 13th Gallium Arsenide and other Compound Semiconductors Application Symposium (GAAS)*, Paris, France, pp. 185-188, 3-4 October 2005.

[4] M. Myslinski, D. Schreurs, and B. Nauwelaers, "Accurate Large-Signal Time-Domain Behavioral Model For Multi-Signal Analysis", *Mikon 2006 16th International Conference on Microwaves, Radar and Wireless Communications*, Cracow, Poland, vol. 3, pp. 977-980, 22-26 May 2006.

[5] D. Schreurs and K. Remley, "Use of multisine signals for efficient behavioural modelling of RF circuits with short-memory effects", *Automatic RF Techniques Group Conference*, pp. 65-72, June 2003.

[6] M. Myslinski, D. Schreurs and B. Nauwelaers, "Influence of Sampling Domain on Behavioral Model Accuracy under Multi-Signal Conditions", *submitted to IEEE T-MTT,* June 2006.

[7] M. Kennel, R. Brown, and H. Abarbanel, "Determining embedding dimension for phase-space reconstruction using a geometrical construction," Phys. Rev. A, pp. 3403-3411, 1992.

[8] Q.J. Zhang and K.C. Gupta, *Neural networks for RF and microwave design*, Artech House, 2000.

[9] D. Schreurs, J. Jargon, K. Remley, D. DeGroot, and K. C. Gupta, "Artificial neural network model for HEMTs constructed from large-signal time-domain measurements," Automatic RF Techniques Group Conf., pp. 31-36, June 2002.

[10] R. Bracewell, *"The Fourier Transform and its Applications, second edition"*, McGraw-Hill, New York, 1986.

[11] J. Wood, J. Horn, and D. Root, "Extending Static Models by using Time Series to Identify the Dynamical Behavior", *Proc. IEEE International Microwave Symposium (IMS)*, Palm Beach (CA), USA, 11-17 June 2005.

[12] D. Schreurs, K.A. Remley and D.F. Williams, "A Metric for Assessing the Degree of Device Nonlinearity and Improving Experimental Design", *IEEE International Microwave Symposium*, Forth Worth, USA, pp. 795-798, 6-11 June 2004.